1-1-2020

Determining the optimal range of coupling coefficient to suppress decline in WPTs efficiency due to increased resistance with temperature rise

Haisen Zhao
North China Electric Power University

Yufei Wang
Chinese Academy of Sciences

Hassan H. Eldeeb
Florida International University

Jiawei Ge
North China Electric Power University

Jinping Kang
North China Electric Power University

See next page for additional authors

Recommended Citation

Authors

Haisen Zhao, Yufei Wang, Hassan H. Eldeeb, Jiawei Ge, Jinping Kang, and Osama A. Mohammed

Determining the Optimal Range of Coupling Coefficient to Suppress Decline in WPTS Efficiency Due to Increased Resistance With Temperature Rise

HAISEN ZHAO [1,2] **(Senior Member, IEEE), YUFEI WANG**[3,4,5] **(Student Member, IEEE),**
HASSAN H. ELDEEB [2] **(Student Member, IEEE), JIAWEI GE**[1]**, JINPING KANG** [1]**,**
AND OSAMA A. MOHAMMED [2] **(Fellow, IEEE)**

[1] School of Electrical and Electronics Engineering, North China Electric Power University, Beijing 102206, China
[2] Department of Electrical and Computer Engineering, Florida International University, Miami, FL 33174 USA
[3] The Key Laboratory of Applied Superconductivity, Chinese Academy of Sciences, Beijing 100190, China
[4] The Institute of Electrical Engineering, Chinese Academy of Sciences, Beijing 100190, China
[5] University of Chinese Academy of Sciences, Beijing 100049, China

CORRESPONDING AUTHOR: JINPING KANG (e-mail: hbdlkjp@163.com).

ABSTRACT The continuous operation of the wireless power transfer system (WPTS) under high-frequency switching activity might cause a temperature rise in various system's components. That temperature rise might increase the resistance of the primary and secondary coils, which will lead to a significant decline in the system's efficiency. To address this problem at the design stage, we investigate the optimal range of the coupling coefficient that suppresses the efficiency drop due to the increasing resistance of the WPTS components. The proposed optimal range of the coupling coefficient can also ensure the output power requirements of the WPTS. Using four different WPTSs, the determination method for the optimal range of coupling coefficients under different system operational frequencies was developed and implemented. A 3-kW resonant experimental prototype WPTS was designed and built to validate the proposed coupling coefficients experimentally. The experimental results show that the optimized coupling range successfully suppressed the efficiency decline resulting from the increasing resistance caused by temperature rise.

INDEX TERMS Wireless power transfer system (WPTS), efficiency, temperature rise, optimal coupling coefficient.

I. INTRODUCTION

With the industrial revolution of electric vehicle (EV) and technological limitations of the battery storage systems, the wireless power transfer system (WPTS) operating at tens of kilohertz represents a perfect candidate for such application [1]–[3]. The WPTS for electric vehicles gained popularity due to their safety, portability and adaptation to harsh conditions. Due to the sensitivity of system efficiency to the operating frequency, electrical circuit topology, and temperature rise, the improvement and stability of system efficiency of WPTS are always the hot issues in this area.

To improve the WPTS's efficiency, two compensation topologies named LC/S [4] and LC/CL [5] were proposed, the number of the coil turns, and the quality factor of the coils was optimized as well in [6]–[7]. Moreover, the performances of the square and circular coils in WPTS were investigated in [8], and the superiority of the square coil in improving system efficiency was revealed [8]. In [9], [10], through the elimination of the ferrite core, the volume, weight, and loss of the loosely coupled transformer (LCT) can be reduced. Similarly, a multi-coil LCT that used only wires and air as a transmission medium was proposed in [11]–[13]. To

minimize the inherent losses of the WPTS DC-DC converters, a dual-side phase shift control method for load modulation and voltage regulation was proposed in [14]. Furthermore, the field-type and non-linear core structures were presented to improve the system's efficiency [3], [15].

For low-power WPTS, the temperature rise caused by power loss is not apparent. However, for the high-power rating ones (i.e., EV applications), the thermal power loss increases the temperature and then inevitably increases the coil resistances. As a result of that temperature-resistance coupled rise, the system's efficiency declines. It was revealed that the change of the original circuit parameters caused by temperature rise would significantly reduce the transmission efficiency [16]. Two methods were proposed in [16] to suppress the decline of system efficiency, including improving coil performance while choosing temperature-robust capacitors, and controlling temperature by applying a heat sink. Furthermore, the thermal characteristics of the magnetic coupler were investigated by simulation [17]. The results showed that the thermal performance of the magnetic coupler could be improved by adequately adjusting the mechanical structure and materials within the allowable range of electrical parameters under the condition of natural cooling.

The efficiency of WPTS in practice may not be as high as expected design due to the uncontrollable operating conditions. Efforts in literature were performed to suppress the decline of system's efficiency. Among the significant factors that contribute to system's efficiency decline is the misalignment of the coils. To ensure the WPTS more tolerant of the coil misalignment, a DD coil structure, namely double D type, was proposed in [18], which can constrain the magnetic flux path and improve the decline of system efficiency to a certain extent. Other structures, including several small, transmit coils that replace the conventional large transmit coil and keep the dimension of the transmitter unchanged was investigated in [19]. Furthermore, a variable inductor (VI) is inserted in the transmitter circuit to compensate extra reactance for enhancing the system's efficiency [20]. In addition, hybrid resonant coils [21] and orthogonal windings [22] show a better tolerance improvement of coil misalignment.

Moreover, previous studies revealed that the slight increase in WPTS components' resistance due to temperature rise would lead to a noticeable decline in the system's efficiency under the prolonged operative time and the high operational frequency conditions [23]. The system's resistance includes the resistance of the coils, the power electronic devices, and the equivalent load. The decline in the system's efficiency due to temperature rise is inevitable. Consequently, it is necessary to find a feasible approach at the design stage to reduce the decline of WPT system's efficiency due to resistance incrimination.

The objective of this study is to present a feasible method to determine, during the design stage, the coupling coefficient range of the WPTS that can suppress the decline in the system's efficiency due to the increase in the system's components resistance. To suppress the decline of system efficiency,
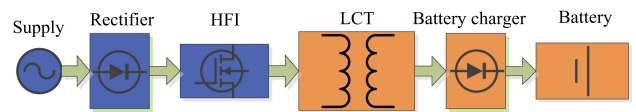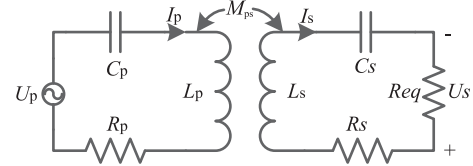

FIGURE 1. Components of WPTS.

FIGURE 2. Equivalent circuit of two-coil WPTS.

this study presents an optimal range of coupling coefficients. The optimized range is capable of diminishing the decline of the system's efficiency and supplying adequate output power from the WPTS. The remainder of this study is organized as follows: Section II investigates the effects of the increased system resistance on its efficiency. Section III proposes the concept of the optimal range of the coupling coefficient and its determination method. Section IV determines the accurate optimal range of coupling coefficient for different WPTSs. In section V, a 3-kW prototype WPTS was manufactured, and the related experiment was also performed to verify the effectiveness of the optimal range of coupling coefficient.

II. INFLUENCE OF INCREASED RESISTANCE ON EFFICIENCY OF WPTS
A. MODEL OF TWO-COIL WPTS
To study the influence of the increased resistance on system's efficiency, a model of a resonant two-coil WPTS is introduced. Fig. 1 shows the components of the resonant two-coil WPTS, it mainly includes the AC supply, rectifier, high-frequency inverter (HFI), loosely coupled transformer (LCT), battery charger and battery. The equivalent circuit of the resonant two-coil WPTS with the series-series (SS) topology is presented in Fig. 2, where U_p is the voltage supply produced by high-frequency inverter (HFI), L_p and L_s are the primary and secondary coil self-inductance, respectively, R_p and R_s are the primary and secondary system resistances, C_p and C_s are the primary and secondary resonant capacitors, respectively, R_{eq} represents the equivalent load resistance, M_{ps} is the mutual inductance of the coils, and ω is the angular frequency of the system. As the WPTS is in resonance, the system output power and efficiency can be expressed as in (1) and (2).

$$P_{out} = \frac{U_p^2 \omega^2 M_{ps}^2 R_{eq}}{\left[R_p\left(R_s + R_{eq}\right) + \omega^2 M_{ps}^2\right]^2} \tag{1}$$

$$\eta = \frac{\omega^2 M_{ps}^2 R_{eq}}{\left[R_p\left(R_s + R_{eq}\right) + \omega^2 M_{ps}^2\right]\left(R_s + R_{eq}\right)} \tag{2}$$

Parameters	Value
Primary voltage U_p (V)	318
Equivalent load resistance R_{eq} (Ω)	28.65
Operating frequency f (kHz)	85
Self-inductance of primary coil L_p (μH)	272.07
Self-inductance of secondary coil L_s (μH)	205.6
Resonant capacitor of primary coil C_p (nF)	12.89
Resonant capacitor of secondary coil C_s (nF)	17.05
Coupling coefficient k_{ps}	0.16

FIGURE 3. Variation of system efficiency with R_p and R_s.

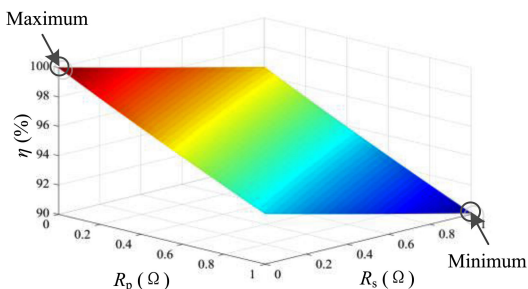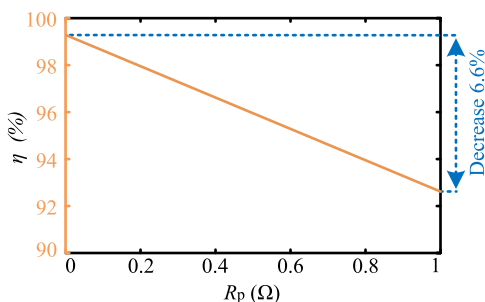FIGURE 4. Variation of system efficiency with Rp.

FIGURE 5. Variation of system efficiency with Rs.

B. EFFECTS OF INCREASED RESISTANCE ON EFFICIENCY OF WPTS

The parameters of a resonant WPTS are displayed in Table 1. According to the previous studies, it was found that only small increments in resistance can affect the system efficiency significantly. Therefore, for direct illustration, it is assumed that the R_p and R_s increase from 0 to 1 Ω, simultaneously, and the conclusion is also suitable to the other WPTS with the different system resistances. The decline in system's efficiency is given in Fig. 3, where the R_p and R_s are the resistances of the primary and the secondary system, respectively. As shown in Fig. 3, the efficiency reaches 100% when the system resistances are 0 Ω (hypothetically), but drops to 90% when the resistances increase to 1 Ω, which means that the system efficiency can drop by 10% when the system resistances increase by 1 Ω.

The variation in efficiency decline is mathematically simulated with the change in R_p and R_s within the aforementioned range. The results displayed in Fig. 4 and Fig. 5 show that, as R_p increases from 0 to 1 Ω, the efficiency decline is linearly
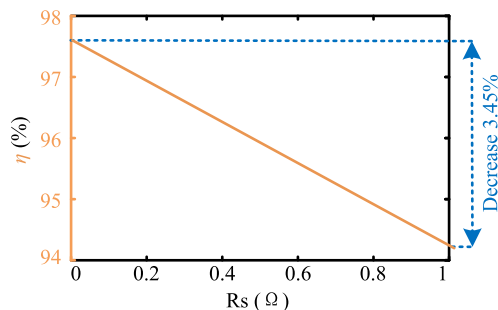
related to the resistance increase, and its maximum reduction percentile was 6.6%, when R_s equals to 1 Ω. And the maximum drop in the system's efficiency was 3.45%, as shown in Fig. 5.

Based on the above analysis, it can be concluded that R_p is a more dominantly active factor in the system's efficiency decline. Consequently, more focus will be highlighted in the next section regarding suppressing the efficiency reduction due to increased R_p.

III. OPTIMAL RANGE OF COUPLING COEFFICIENT FOR SUPPRESSING DECLINE OF EFFICIENCY
A. VARIATIONS OF SYSTEM OUTPUT POWER AND EFFICIENCY WITH THE COUPLING COEFFICIENT
In order to serve the global study's objective of minimizing the reduction in the WPTS's efficiency due to increased R_p, the variations of output power and efficiency with the coupling coefficient between the primary and secondary coils, k_{ps}, are introduced, as shown in Fig. 6. It shows the variations of the output power and system's efficiency for four different WPTSs under various values of R_p. The parameters of four WPTSs are listed in Table 2, and Fig. 6(a), (b), (c), and (d) are the calculated results for cases 1 to 4, respectively. The selection of the four specific cases (i.e., cases 1-4 [24]) presented in Table 2 is for a general interpretation of the optimal coupling range determination approach. Furthermore, the cases mentioned in the above studies are commonly adopted in the literature. The resistances of the primary system are R_{p1}, R_{p2}, and R_{p3} ($R_{p2} = 2R_{p1}$ and $R_{p3} = 3R_{p1}$).

As shown in Fig. 6(a) to (d), the system's efficiency increases sharply then smoothly with the increase of k_{ps}. While the output power increases until specific values of k_{ps} then fall down to almost zero. Moreover, it is noticeable from the figures that the different values of R_p do not play a vital role in changing the system's efficiency or output power with the rise in k_{ps}. From the previous observations, it can be concluded that:

1) The decline in the system's efficiency due to increased resistance can be overcome by increasing the coupling coefficient of WPTS.
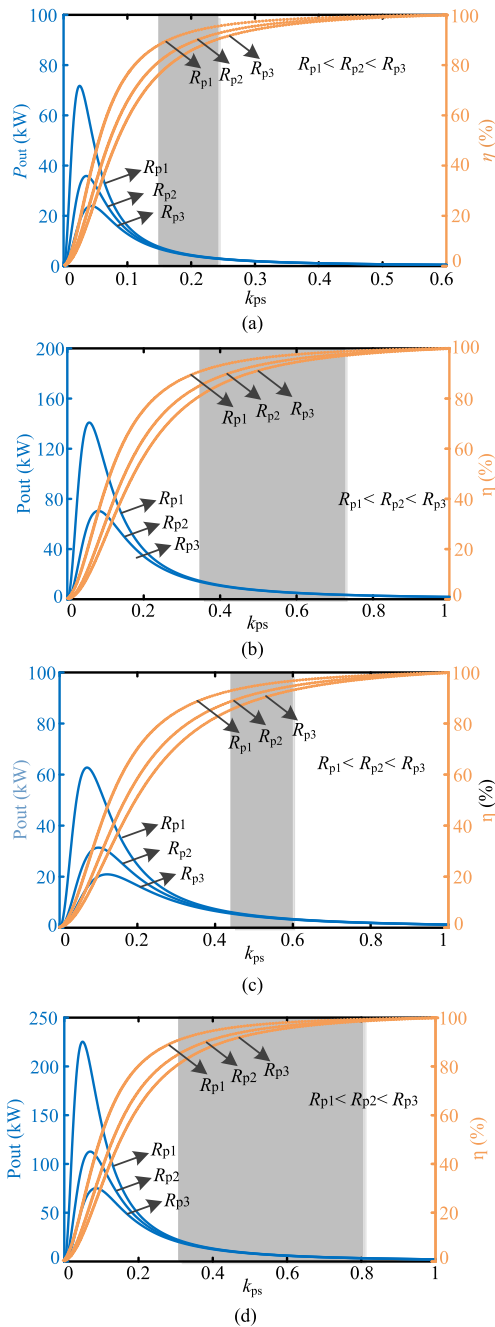
FIGURE 6. Variations of efficiency and output power with coupling coefficient under different primary resistances (a) case 1, (b) case 2, (c) case 3, (d) case 4.

2) The coupling coefficient of the system should be reasonably significant in order to enhance the system's efficiency without reducing the output power capability.

B. CONCEPT OF OPTIMAL RANGE OF COUPLING COEFFICIENT

Based on the above analysis, the optimal range of k_{ps} that counter-balances the reduction in the system's efficiency due to the rise in the WPTS's resistance without violating the

TABLE 2 Parameters of Four Different WPTSs

Parameters	Case 1	Case 2	Case 3	Case 4
Primary voltage U_p (V)	318	195	150	236
Equivalent load resistance R_{eq} (Ω)	28.65	4	2	2
Operating frequency f (kHz)	85	25	25	25
Self-inductance of primary coil L_p (μH)	272.07	56.41	38.2	45.51
Self-inductance of secondary coil L_s (μH)	205.6	58.69	38.17	45.19
Primary resonant capacitor C_p (nF)	12.89	718.46	1060.95	890.54
Secondary resonant capacitor C_S (nF)	17.05	690.55	1061.79	896.85
Primary resistance R_p (Ω)	0.35	0.0665	0.0865	0.0601
Secondary resistance R_s (Ω)	0.2	0.0591	0.0727	0.0565
Coupling coefficient k_{ps}	0.16	0.254	0.231	0.162

TABLE 3 Optimal Ranges of Coupling Coefficient in Different WPTSs Under Different Frequencies

Case	System operating frequency f (kHz)	Optimal range of coupling coefficient
1	85	0.15~0.23
2	25	0.36~0.73
3	25	0.44~0.6
4	25	0.31~0.8

output power capability of the system is introduced. Finding the optimal range of the coupling coefficient is confined via two constraints. Firstly, the efficiency decline due to resistance increase does not fall beyond a given minimum value determined by the designer to determine the lower limit of the coupling ranges. Secondly, the system's output power does not exceed the required value to determine the upper limit of the ranges.

Considering case 1, the relations of (1) and (2) are the objective functions to be maximized under the constraints of (3) and (4), in which threshold value "5%" and "3.3 kW" are determined by the actual requirement. Afterward, the optimal range of k_{ps}, under 85-kHz operational frequency, can be confined within the grey area in Fig. 6(a). The coupling coefficients in that area can ensure the system's efficiency and output power constraints in (3) and (4), respectively.

$$\frac{\eta_{R_{p1}} - \eta_{R_{p3}}}{\eta_{R_{p1}}} \times 100\% \leq 5\% \tag{3}$$

$$P_{out} \geq 3.3 \tag{4}$$

Similarly, the optimal range of coupling coefficient of the other cases operating at 25 kHz can also be obtained, as shown in the highlighted areas in Fig. 6(b), (c) and (d), respectively. The optimal ranges of the coupling coefficient are shown in Table 3. It can be concluded from the table that the coupling coefficients are inversely proportional to the operational frequency. For instance, the optimal range of k_{ps} is from 0.15 to 0.23 at 85 kHz, while it is from 0.31 to 0.8 for the 4th case at 25 kHz.

With the efficiency relation displayed in (2), the relationship of the coupling coefficient with the frequency can be obtained when the overall efficiency of the system is kept unchanged; the result is shown in Fig. 7. It depicts that k_{ps}
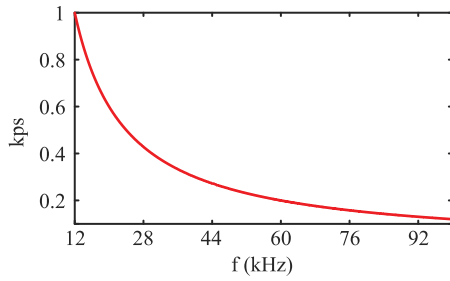
FIGURE 7. Relationship of coupling coefficients and operating frequency.

is inversely proportional to the operational frequency for a given output system's efficiency. Thereby, a system operating frequency is uniquely correspondent to a coupling coefficient. In other words, for a given system, the optimal range of k_{ps} changes as the operational frequency of the WPTS alters. Moreover, as the data of cases, 2 to 4 in Table 3 show that the system operating frequencies of these cases is 25 kHz, and that the values of k_{ps} from 0.44 to 0.6 can satisfy the optimality requirement for all the three cases. Therefore, it can also be inferred that the optimal ranges of the coupling coefficient of different systems at the same frequency may be the same.

From the presented analysis, the optimal ranges of the coupling coefficient under different operational frequencies will be determined in the following section.

IV. DETERMINATION APPROACH OF THE OPTIMAL RANGE OF COUPLING COEFFICIENT

In this section, the optimal ranges of coupling coefficients are analyzed and obtained when the operating frequency is 25 kHz, 55 kHz, and 85 kHz, respectively. Here, the operating frequency 85 kHz and 25 kHz are adopted in [2], [11], [24]. Furthermore, it is found that there may be overlapping areas of coupling coefficient range under different operation frequencies, to effectively distinguish the optimal coupling coefficient range under different operating frequencies, an intermediate frequency, 55 KHz, is selected between 25 kHz and 85 kHz. And the results are presented in Fig. 8.

With case 1 in section III, the approach to determining the optimal ranges of coupling coefficient under different operational frequencies is as follows.

1) Table 3 shows that the optimal range of coupling coefficient for case 1 at 85 kHz is 0.15 to 0.23. The system's efficiency at the lower limit of the optimal range of the coupling coefficient is 96.59% when the primary resistance of case 1 equals R_{p1}. Whereas the system's output power at the upper limit of the optimal range of the coupling coefficient is 3.3 kW.

2) As shown in Fig. 8(a), two horizontal lines are drawn at $\eta = 96.59\%$ and $P_{out} = 3.3$ kW to represent the benchmarks of the determination process. The first horizontal line intersects with the system efficiency curves of 85 kHz, 55 kHz, and 25 kHz at points A, C and E, respectively. The second horizontal line intersects
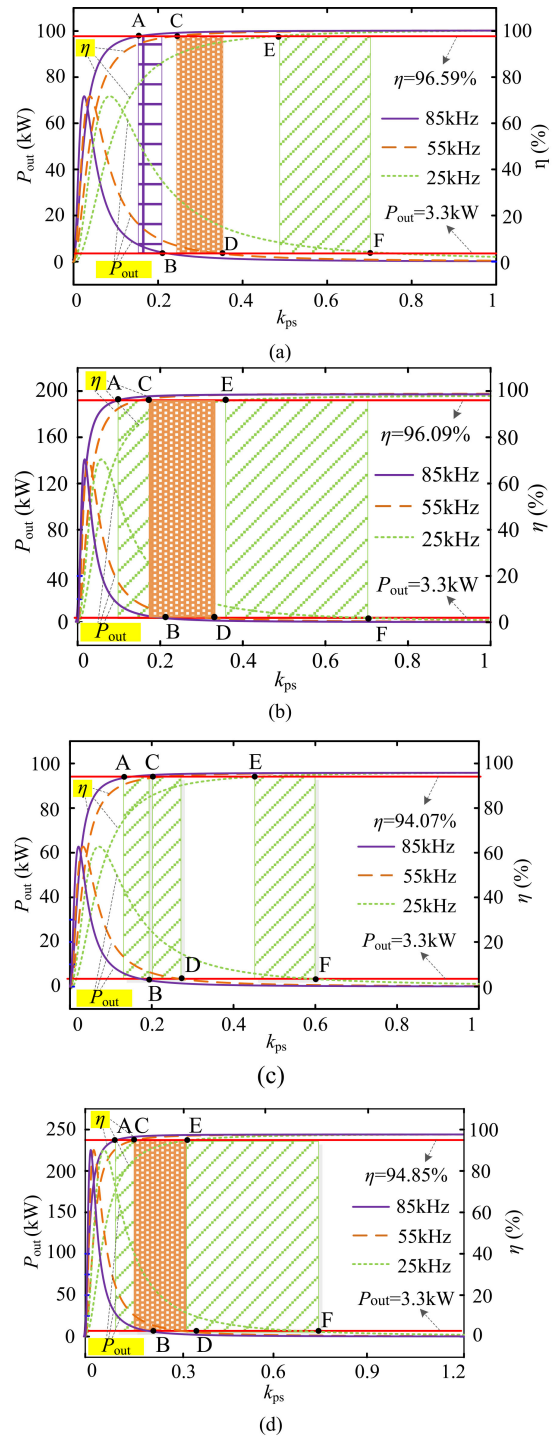
FIGURE 8. Variations of the system efficiency and output power with coupling coefficient and system operating frequency (a) case 1, (b) case 2, (c) case 3, (d) case 4.

with the output power curves of 85 kHz, 55 kHz, and 25 kHz at points B, D, and F, respectively. The ranges determined by the horizontal line of A and B, C, and D, as well as E and F are defined as the optimal ranges of coupling coefficient at 85 kHz, 55 kHz, and 25 kHz, respectively.

TABLE 4 Optimal Ranges of Coupling Coefficient for Different System Operating Frequencies in Different Systems

Case	25 kHz	55 kHz	85 kHz
1	0.51-0.78	0.24-0.35	0.15-0.23
2	0.36-0.73	0.17-0.33	0.11-0.21
3	0.44-0.6	0.2-0.27	0.13-0.18
4	0.31-0.8	0.15-0.36	0.1-0.23

TABLE 5 Optimal Ranges of Coupling Coefficient Under Different System Operating Frequencies

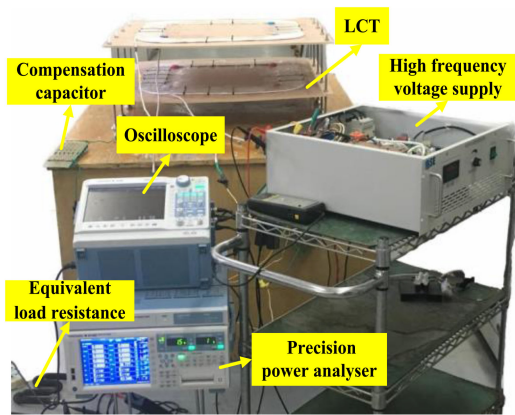| Operating frequency	Optimal range of coupling coefficient
25 kHz	0.51-0.6
55 kHz	0.24-0.27
85 kHz	0.15-0.18

FIGURE 9. Two-coil WPTS test rig.

Similarly, the optimal ranges of the coupling coefficient of the other cases can also be obtained, as shown in Fig. 8(b) to (d), respectively.

Due to stringent efficiency and output power requirements of various WPTSs, the overlapping areas at the different operation frequencies cannot be avoided, as shown in Fig. 8(b) and Fig. 8(d), but it does not affect the results of optimal ranges of coupling coefficient at a given operational frequency.

The specific values of optimal ranges of k_{ps} for the four cases at different operational frequencies are given in Table 4. Afterward, the typical sections of the k_{ps} optimal ranges are obtained and shown in Table 5.

As the operational frequency of WPTS is usually close to 85 kHz, in the following section, the effectiveness of the optimal range of the coupling coefficient is experimentally verified at 85 kHz, for suppressing the efficiency decline caused by the resistance escalation.

V. EXPERIMENT VALIDATION

A. DESIGN AND ESTABLISHMENT OF A TEST RIG

To verify the applicability of the previously presented investigation, a 3-kW two-coil prototype WPTS was designed and manufactured to perform the experimental studies. as shown in Fig. 9. According to the descriptions in Fig. 1, the design
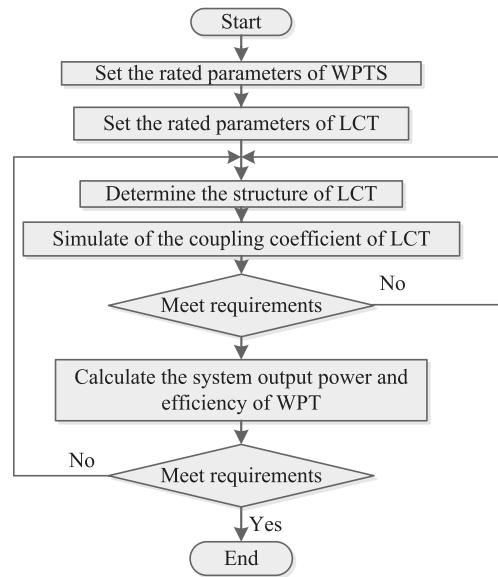

FIGURE 10. Design flow chart of two-coil prototype WPTS.

steps of WPTS with SS topology can be summarized as shown in Fig. 10. *And the specific steps involved in the design of WPTS are as follows.*

Step 1: Set the desired rated values of the output power and efficiency of the WPTS.

Step 2: Define the rated values of the coupling coefficient and the air gap of the LCT.

Step 3: Determine the dimensions of LCT, the coils' number of turns, and the arrangement of wires.

Step 4: Establish the 3-D finite element (3D-FE) simulation model of the designed LCT and calculate the self- and mutual inductance of coils. Determine whether the coupling coefficient of the LCT meets the criteria of the rated coupling coefficient in step 2. If yes, execute the next step. If not, return to step 3.

Step 5: Substitute the self-inductance and mutual inductance of coils into (1) and (2) to calculate the system's output power and efficiency. Determine whether the output power and efficiency of the WPTS meet the rated values in step 1. If yes, execute the next step. If not, return to step 3.

Step 6: Manufacture the prototype WPTS.

The test rig of WPTS is established, and the system specifications are given in Table 6. This test rig mainly composed of a high-frequency supply, two sets of compensation capacitors, a resistance load and a LCT. The size of developed LCT is 700 mm × 700 mm × 6.5 mm, the primary and secondary coils are made by standrized Litz wires (0.1 mm × 2000), which can reduce the skin effect effectively. It is noticed that to avoid the high-frequency radiation, an aluminum plate is adopted as the shielding in the experiment. Furthermore, to prevent excessive temperature rise, natural air cooling and forced air cooling are selected for the LCT and the load resistance, respectively.

TABLE 6 Specifications of Prototype

Parameters	Measured value
Primary voltage U_p (V)	285
Turns of the primary coil	16
Turns of the secondary coil	16
Operating frequency f (kHz)	85
Self-inductance of primary coils L_p (μH)	336.5
Self-inductance of secondary coils L_s (μH)	337.133
Primary resonant capacitor C_p (nF)	11.306
Secondary resonant capacitor C_s (nF)	11.28
Equivalent load resistance R_{eq} (Ω)	47.4

TABLE 7 Experimental Results

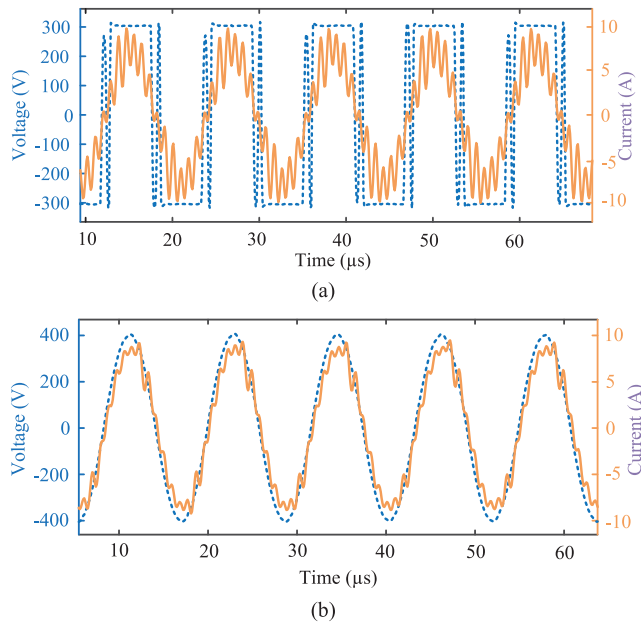| Case	k_{ps}	R_s (Ω)	η (%)	P_{out} (kW)	η_{md} (%)
1	0.118	48.735	91.302	3.387	19.065
		49.012	84.775	3.188	
		49.106	72.237	2.729	
2	0.132	48.765	94.672	2.696	16.717
		49.019	90.191	2.624	
		49.17	77.955	2.392	
3	**0.165**	**48.778**	**98.317**	**1.696**	**5.264**
		49.012	**97.203**	**1.747**	
		49.101	**93.053**	**1.779**	
4	0.232	49.15	99.092	1.314	3.968
		49.723	97.717	1.326	
		49.892	95.124	1.63	

FIGURE 11. Tested waveforms in resonance condition. (a) primary voltage and current. (b) Secondary voltage and current.

The inductance and resistance of the two LCT's coils are measured using a precise impedance analyzer; other parameters such as system output power and efficiency are measured by a precise power analyzer. Furthermore, the waveforms of the voltage and current of the prototype are recorded by a digital oscilloscope. At the resonance situation, the voltage and current waveforms of the primary and secondary systems are shown in Fig. 11(a) and Fig. 11(b). The zero phase angle between the waveforms shown in Fig. 11 suggests that the system is resonating.

B. EXPERIMENTAL RESULTS

Using the experimental test bench, the system's output power and efficiency can be measured for the four different coupling coefficients when the system's resistance increases by a similar extent. Afterward, the maximum decline in system's efficiency, η_{md}, under various loading conditions were computed and displayed in Table 7. It is worthy of mentioning that R_s is the whole system's resistance. As seen in Table 7, it can be concluded that:

1) When k_{ps} rises from 0.118 to 0.232, the maximum of the system efficiency rises from 91.302% to 99.092%, and the maximum of the system output power drops from 3.387 kW to 1.63 kW. Therefore, it can be concluded that the system's efficiency increases with the increment of k_{ps}. However, the system's output power decreases gradually. This conclusion is consistent with the theoretical analysis in section III and the trends shown in Section III.

2) When k_{ps} is 0.118 (less than the lower limit of the optimal range of coupling coefficient at 85 kHz), η_{md} drops to 19.065%, and the system's output power becomes almost 3 kW. Moreover, with $k_{ps} = 0.165$, the efficiency of WPT system decreases from 98.317% to 93.053% when system's resistance increases from 48.778 to 49.101 Ω, which is higher than that of cases 1 and 2. Meanwhile, η_{md} in case 3 is only 5.264%, which shows the system efficiency decline can be significantly reduced to only 27% of that in case 1. Therefore, it can be concluded that the optimal range of coupling coefficient can suppress the decline of the system efficiency effectively. That conclusion agrees with the theoretical analysis presented in Section III. With the further escalation in the coupling coefficient, until it exceeds the upper limit of the optimal range at 85 kHz (as shown in case 4), the system output power drops from around 1.7 kW to around 1.3 kW, which cannot meet the practical system's requirements. Therefore, it can also be concluded that the optimal range of the coupling coefficient can ensure the sufficient system's output power.

3) When k_{ps} is equal to 0.118 and 0.132, respectively, the system's output power gradually decreases with the increase of the system resistance. However, when k_{ps} is equal to 0.165 and 0.232, respectively, with the rise in the system resistance, the system's output power gradually increases. That observation reinforces the trends of the system's output power shown in Fig. 12. As shown in Fig. 12, with the increase of the system resistance, the system efficiency gradually decreases regardless of the value of the coupling coefficient. However, the system's output power decreases and then increases gradually,
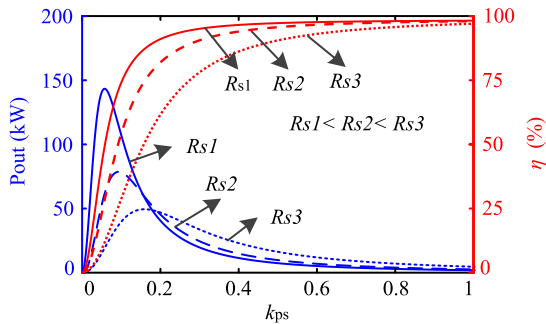
FIGURE 12. Variations of system output power and efficiency with coupling coefficient under different system resistances.

which results from the increase of the coupling coefficient of the system beyond a particular value.

To sum up, the proposed optimal range of coupling coefficient can suppress the decline of system efficiency when the resistance increases due to temperature rise.

VI. CONCLUSION

This study presents an optimal range of coupling coefficient for suppressing the decline of WPTS caused by the increased system's resistance due to temperature rise. The main contributions are as follows:

1) The influence of the increased resistance on the WPTS's efficiency was investigated. It was revealed that the increasing resistance in the primary coil could lead to more significant efficiency decline in a two-coil resonant WPTS

2) Optimal range of coupling coefficient was proposed to suppress the efficiency decline at the design stage. That range ensured that: A) the degree of the system efficiency reduction can be reduced to less than 5 percentage points, and B) no violation of the system's output power requirement.

3) A 3-kW resonant WPTS was designed, and a prototype was also manufactured. Experimental validations were carried out by operating the system under different coupling coefficient. It was shown that the efficiency decline of WPTS could be reduced effectively with the presented optimal range of the coupling coefficient. Moreover, the study presented a systematic approach for WPTS developers to select the optimal coupling range for any given WPTS.

REFERENCES

[1] H. H. Eldeeb, A. T. Elsayed, C. R. Lashway, and O. Mohammed, "Hybrid energy storage sizing and power splitting optimization for plug-in electric vehicles," *IEEE Trans. Ind. Appl.*, vol. 55, no. 3, pp. 2252–2262, May/Jun. 2019.

[2] G. Buja, M. Bertoluzzo, and K. N. Mude, "Design and experimentation of WPT charger for electric city car," *IEEE Trans. Ind. Electron.*, vol. 62, no. 12, pp. 7436–7447, Dec. 2015.

[3] Z. J. Li, C. B. Zhu, J. H. Jiang, K. Song, and G. Wei, "A 3-kW wireless power transfer system for sightseeing car supercapacitor charge," *IEEE Trans. Power Electron.*, vol. 32, no. 5, pp. 3301–3316, May 2017.

[4] Y. J. Wang, Y. S. Yao, X. S. Liu, D. G. Xu, and L. Cai, "An LC/S compensation topology and coil design technique for wireless power transfer," *IEEE Trans. Power Electron.*, vol. 33, no. 3, pp. 2007–2025, Mar. 2018.

[5] Y. S. Yao, X. S. Liu, Y. J. Wang, and D. G. Xu, "LC/CL compensation topology and efficiency-based optimization method for wireless power transfer," *IET Power Electron.*, vol. 11, no. 6, pp. 1029–1037, May 2018.

[6] Q. J. Deng *et al.*, "Frequency-dependent resistance of litz-wire square solenoid coils and quality factor optimization for wireless power transfer," *IEEE Trans. Ind. Electron.*, vol. 63, no. 5, pp. 2825–2837, Dec. 2016.

[7] G. Q. Zhu and R. D. Lorenz, "Achieving low magnetic flux density and low electric field intensity for a loosely coupled inductive wireless power transfer system," *IEEE Trans. Ind. Appl*, vol. 54, no. 6, pp. 6383–6393, Nov./Dec. 2018.

[8] Z. C. Luo and X. Z. Wei, "Analysis of square and circular planar spiral coils in wireless power transfer system for electric vehicles," *IEEE Trans. Ind. Electron.*, vol. 65, no. 1, pp. 331–341, Jul. 2018.

[9] W. Zhang, J. C. White, A. M. Abraham, and C. C. Mi, "Loosely coupled transformer structure and interoperability Study for EV wireless charging systems," *IEEE Trans. Power Electron.*, vol. 30, no. 11, pp. 6356–6367, May 2015.

[10] A. A. S. Mohamed and O. Mohammed, "Physics-based co-simulation platform with analytical and experimental verification for bidirectional IPT system in EV applications," *IEEE Trans. Veh. Technol.*, vol. 67, no. 1, pp. 275–284, Jan. 2018.

[11] D. H. Tran, V. B. Vu, and W. Choi, "Design of a high-efficiency wireless power transfer system with intermediate coils for the on-board chargers of electric vehicles," *IEEE Trans. Power Electron.*, vol. 33, no. 1, pp. 175–187, Feb. 2018.

[12] F. P. Wijaya, T. Shimotsu, T. Saito, and K. Kondo, "A simple active power control for a high-power wireless power transmission system considering coil misalignment and its design method," *IEEE Tran. Power Electron.*, vol. 33, no. 11, pp. 9989–10002, Nov. 2018.

[13] S.-C. Moon and G.-W. Moon, "Wireless power transfer system with an asymmetric four-coil resonator for electric vehicle battery chargers," *IEEE Tran. Power Electron.*, vol. 31, no. 10, pp. 6844–6854, Dec. 2016.

[14] X. Liu, T. F. Wang, and X. J. Yang, "Analysis of efficiency improvement in wireless power transfer system," *IET Power Electron.*, vol. 11, no. 2, pp. 302–309, Apr. 2018.

[15] M. Mohammad, S. Choi, Z. Islam, S. Kwak, and J. Baek, "Core design and optimization for better misalignment tolerance and higher range of wireless charging of PHEV," *IEEE Trans. Transp. Electrific.*, vol. 3, no. 2, pp. 445–453, Jun. 2017.

[16] K. Hwang, S. Chun, U. Yoon, M. Lee, and S. Ahn, "Thermal analysis for temperature robust wireless power transfer systems," in *Proc. IEEE Wireless Power Transfer*, Perugia, Italy, May 2013, pp. 52–55.

[17] C. B. Zhu *et al.*, "Thermal simulation and optimization study for magnetic coupler of static electric vehicle wireless power transfer systems," in *Proc. 22nd Int. Conf. Elect. Mach. Syst.*, Harbin, China, Aug. 2019, pp. 1–4.

[18] M. Budhia, J. T. Boys, G. A. Covic, and C. Y. Huang, "Development of a single-sided flux magnetic coupler for electric vehicle IPT charging systems," *IEEE Trans. Ind. Electron.*, vol. 60, no. 1, pp. 318–328, Dec. 2013.

[19] X. L. Mou, O. Groling, and H. J. Sun, "Energy efficient and adaptive design for wireless power transfer in electric vehicles," *IEEE Trans. Ind. Electron*, vol. 64, no. 9, pp. 331–341, Sep. 2017.

[20] W. X. Zhong and S. Y. R. Hui, "Maximum energy efficiency operation of series-series resonant wireless power transfer systems using on-off keying modulation," *IEEE Trans. Power Electron.*, vol. 33, no. 4, pp. 3595–3603, Apr. 2018.

[21] Q. W. Zhu, Y. J. Guo, L. F. Wang, C. L. Liao, and F. Li, "Improving the misalignment tolerance of wireless charging system by optimizing the compensate capacitor," *IEEE Trans. Ind. Electron.*, vol. 62, no. 8, pp. 4832–4836, Aug. 2015.

[22] F. Y. Lin, S. Kim, G. A. Covic, and J. T. Boys, "Effective coupling factors for series and parallel tuned secondaries in IPT systems using bipolar primary pads," *IEEE Trans. Transp. Electrific.*, vol. 3, no. 2, pp. 434–444, Jun. 2017.

[23] M. Alsayegh, S. Mohannad, M. Clemens, and B. Schmuelling, "Magnetic and thermal coupled field analysis of wireless charging systems for electric vehicles," *IEEE Trans. Magn.*, vol. 55, no. 6, Jun. 2019, Art. no. 7400704.

[24] J. Jia, H. Omori, M. Tsuno, T. Morizane, N. Kimura, and M. Nakaoka, "A comparative study on efficiency and leakage magnetic field of transfer coils with different structures in a magnetic resonant WPT system," in *Proc. IEEE 2nd Annu. Southern Power Electron. Conf.*, Auckland, 2016, pp. 1–6.

JIAWEI GE was born in Jiangsu, China, in 1995. He received the B.E. degree in automation from Hebei University, Baoding, China, in 2017. Since 2018, he has been working toward the M. Eng. degree in electrical engineering with North China electric University, Beijing, China. His research interests includes wireless power transfer.

JINPING KANG was born in Shanxi, China, in 1975. She received the B.E. degree in power system and automation from Taiyuan University of Technology, Taiyuan, China, in 1996, and the M.E. and Ph.D. degrees in electric machines and apparatus from North China Electric Power University, Beijing, China, in 1999 and in 2010, respectively. She is currently an Associate Professor with the School of Electrical and Electronics Engineering, North China Electric Power University, Beijing, China. Her research interests include modeling of electrical machines and wireless power transfer.

OSAMA A. MOHAMMED (Fellow, IEEE) received the master's and doctoral degrees in electrical engineering from Virginia Tech, Blacksburg, VA, USA, in 1981 and 1983, respectively. He is currently a Distinguished Professor and the Associate Dean of Research at the College of Engineering, Florida International University (FIU), Miami, FL, USA. He is also the Director of the Energy Systems Research Laboratory, FIU and a Professor of electrical and computer engineering. He is a world-renowned expert on various topics in power and energy systems, including design optimization and physics-based modeling in electric machines and drives, energy storage systems, and power electronics. He currently has active research projects for several federal agencies in these areas. Additionally, he has research interests in smart-grid distributed control, interoperability, and energy cyber-physical systems. His presentations are frequently invited at academic and industrial organizations and conferences worldwide. He has authored or coauthored more than 750 articles in refereed journals and international conferences and holds 16 patents awarded or filed. He has also authored a book and several book chapters. He is also an Elected Fellow of the Applied Computational Electromagnetic Society ACES. He was the recipient of the prestigious IEEE Power and Energy Society Cyril Veinott Electromechanical Energy Conversion Award and the 2012 Outstanding Research Award from FIU, the 2017 Outstanding Doctoral Mentor, and the Distinguished Professor designation in 2018.

HAISEN ZHAO (Senior Member, IEEE) was born in Hebei, China, in 1982. He received the B.E. degree in agricultural electrification and automation from Agriculture University of Hebei, Baoding, China, in 2004, and the M.E. and Ph.D. degrees in electric machines and apparatus from North China Electric Power University, Beijing, China, in 2007 and in 2011, respectively. He is currently an Associate Professor with the School of Electrical and Electronic Engineering, North China Electric Power University. He was a Visiting Scholar with the Energy Systems Research Laboratory, Department of Electrical and Computer Engineering, Florida International University, Miami, FL, USA, from December 2018 to December 2019. He is the author or coauthor of more than 100 articles in peer-reviewed journals and major international conferences. Furthermore, he has 15 patents awarded in the related area. His research interests include electrical motors design, energy saving technologies of electric machines and wireless power transfer.

YUFEI WANG (Student Member, IEEE) was born in Shandong, China, in 1992. He received the B.E. degree in electrical engineering and automation from Shandong University of Science and Technology, Qingdao, China, in 2014, and the M.E. degree in electric machines and apparatus from North China Electric Power University (NCEPU), Beijing, China, in 2019. He is currently working toward the Ph.D. degree with the Institute of Electrical Engineering, Chinese Academy of Sciences, Beijing, China. His research interest is wireless power transfer.

HASSAN H. ELDEEB (Student Member, IEEE) received the B.Sc. (with first class Hons.) and M.Sc. degrees in electrical power and machine engineering from Ain Shams University, Cairo, Egypt, in 2011 and 2016, respectively, and the M.Sc. degree in electrical engineering in 2019 from Florida International University, Miami, FL, USA, where he is currently working toward the Ph.D. degree. He is the author or coauthor of more than eight articles in IEEE Journals and 25 papers at major international conferences. His research interests include real-time diagnosis, control, and design of electric machines and motors drives. He holds one patent awarded from the US Patents Service Office in the area of electric drives diagnosis. He was the recipient of the Outstanding Presentation Award at the IEEE Applied Power Electronics Conference (APEC) 2019, Anaheim, CA, USA, in March 2019, and the Best Student Poster Award at the 53rd IEEE IAS Annual Meeting CMD Poster Contest, Portland, OR, USA, in September 2018. He is a topic chair at the 2020 IEEE Energy Conversion Congress & Expo, Detroit, MI, USA October 2020. Moreover, he was the Chair of the Poster Contest at the 54th IEEE IAS 2019 CMD Annual Workshop, Baltimore, MD, USA, September 2019. He has been the Secretary of the IEEE IAS chapter of the Miami Section since January 2019.